IEEE Photonics Journal
An IEEE Photonics Society Publication

Open Access

Parasitic Stimulated Amplification in High-Peak-Power and Diode-Seeded Nanosecond Fiber Amplifiers

Volume 6, Number 3, June 2014

C. L. Chang
P. Y. Lai
Y. Y. Li
Y. P. Lai
C. W. Huang
S. H. Chen
Y. W. Lee
S. L. Huang, Senior Member, IEEE

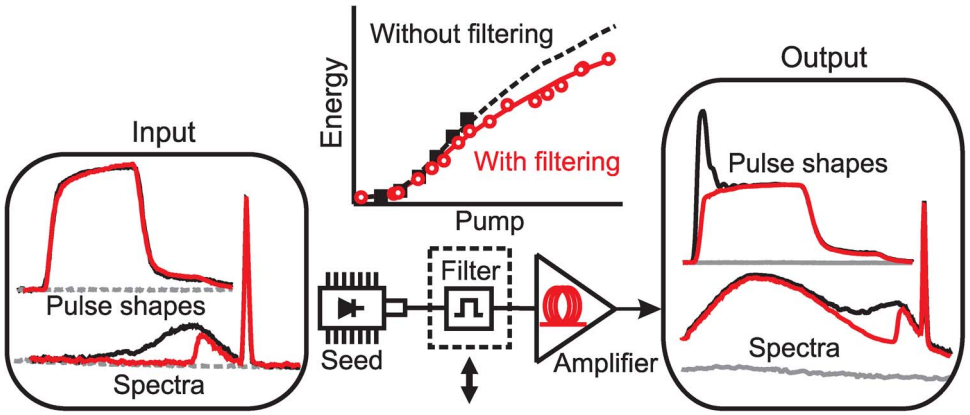

DOI: 10.1109/JPHOT.2014.2319090
1943-0655

IEEE photonics SOCIETY

IEEE

Parasitic Stimulated Amplification in High-Peak-Power and Diode-Seeded Nanosecond Fiber Amplifiers

C. L. Chang,[1] P. Y. Lai,[2] Y. Y. Li,[1] Y. P. Lai,[1] C. W. Huang,[1] S. H. Chen,[2] Y. W. Lee,[3] and S. L. Huang,[1,4] *Senior Member, IEEE*

[1]Institute of Photonics and Optoelectronics, National Taiwan University, Taipei 10617, Taiwan, and also with Research Laboratory of Electronics, Massachusetts Institute of Technology, Cambridge, MA 2131-4307, USA
[2]Department of Physics, National Central University, Jhongli 32001, Taiwan
[3]Department of Electro-Optical Engineering, National Taipei University of Technology, Taipei 10608, Taiwan
[4]Department of Electrical Engineering, National Taiwan University, Taipei 10617, Taiwan

DOI: 10.1109/JPHOT.2014.2319090

Manuscript received March 16, 2014; revised April 14, 2014; accepted April 14, 2014. Date of publication April 23, 2014; date of current version May 5, 2014. This work was supported by the National Science Council, Taiwan, under Grants NSC-101-2120-M-002-006 and NSC-101-2112-M-008-012. The National Center for High-Performance Computing, Taiwan provided resources under the national project "Taiwan Knowledge Innovation National Grid." C.-L. Chang was supported by a scholarship provided by National Defense Industrial Development Foundation. Corresponding author: S. L. Huang (e-mail: shuang@ntu.edu.tw).

Abstract: The broadband parasitic amplification in a diode-seeded nanosecond ytterbium-doped fiber laser amplifier system is numerically and experimentally investigated. The amplification is originated from a weak and pulsed parasitic signal associated with the 1064-nm seed diode laser. Although the average power of the parasitic pulse is less than 5% of the total seed laser power, a significant transient spike is observed during the amplification. In agreement with the simulation, nonlinear effects caused by the transient spike limits the scaling of signal peak power in fiber preamplifiers. With the utilization of a narrow bandwidth filter to eliminate the parasitic pulse, the power and energy scalability of a multistage diode-seeded fiber amplifier laser system has been significantly improved. At 1064 nm, pulses with the peak power of 120 kW and energy of 1.2 mJ have been successfully generated in the multistage Yb^{3+}-doped fiber amplifier with an energy gain of 63 dB and 56% conversion efficiency. In viewing of the parasitic pulse's 8.8-nm bandwidth, it has the potential to become a novel seed source for high-peak-power fiber amplifiers.

Index Terms: Fiber lasers, laser amplifiers, diode lasers, coherent sources modeling and theory, novel photon sources, pulse shaping.

1. Introduction

Rare-earth-doped fiber lasers are successful to produce efficient, stable, and high quality laser beams in alignment-free configurations with compactness and robustness [1]. In recent years, high-power pulsed fiber laser systems have facilitated wide spread applications in academics, industries, and militaries in replacement of conventional bulk solid-state laser systems. The utilization of amplifier configurations can avoid the high intra-cavity power density which limits the power scaling of a single-stage Q-switched or gain-switched nanosecond fiber laser. In order to alleviate signal saturation of a single-stage amplifier [2], the pulse energy, peak power [3], or average power [4] have been scaled up using fiber amplifier cascades or the so-called configuration of master oscillator power amplifier (MOPA). It is composed of a highly controlled seed, high-gain preamplifiers, and high-efficiency

power amplifiers. A directly modulated nanosecond laser diode can provide a highly-controlled seed with the flexibility in terms of output parameters, such as repetition rate, pulse duration, and temporal shape. However, the attainable peak power of such a seed diode is usually low if more advanced performances are required such as single transverse mode, single frequency, fast rise/fall time, and so on [5]. Therefore, the design of high-gain preamplifier becomes critical for efficient scaling of the diode-seeded MOPA scheme to high power or high energy.

In previous studies, a transient spike emerges at the leading edge of the amplified pulse during the amplification process before signal saturation [2]. Such an unexpected spike at the leading edge of a laser pulse may be harmful in laser guidance, communication, and range finding, in which it will lead to a higher error rate due to the pulse distortion. Furthermore, the peak power of this leading spike rather than the signal pulse is easy to exceed the nonlinear thresholds [6] and even the damage threshold [7] of fiber amplifiers. As a result, the attainable peak power or pulse energy generated by the amplifier system is limited, especially by fiber preamplifiers. The undesired spike formation has been reported [8], [9]. Through adaptive pulse shaping technique based on electro-optic modulator [8], it can be eliminated by shaping the output pulse of seed diode laser before entering the MOPA system. In addition, an approach based on the nonlinear polarization rotation by optical Kerr effect [10] was proposed to suppress the transient spike propagating in a non-polarization-maintaining (non-PM) fiber. Because the leading spike was stripped after coupling the amplified laser pulse out from the MOPA system, power or energy scaling is still limited. Though deformation of pulse shape during propagation in a fiber may be induced by nonlinear effects, e.g. the dynamic behavior of stimulated Brillouin scattering [11] or the self-steeping effect in femtosecond regime [12], for a diode-seeded MOPA system, there is no sufficient experimental evidence or numerical analysis to clarify both origin and formation of the transient spike. The leading spike was believed to be induced by the noise which is originated from the relaxation oscillations of the gain-switched seed sources [10] or the gain-switched fiber lasers [13]. So far, a number of fiber MOPAs have generated high power nanosecond pulses [14]–[16].

In this paper, we study both experimentally and numerically the formation of the transient spike in a diode-seeded fiber MOPA system. A numerical code based on multi-wavelength and distributed interactions was developed to simulate the pulsed signal amplification with the consideration of the parasitic amplification and the cw amplification spontaneous emission. The simulation results agree well with the experimental results. The gain dependence of the spike formation was investigated by varying pump power, central wavelength, spectral bandwidth, active fiber length, and repetition rate. By eliminating the seed noise, the amplified spike was suppressed in the core-pumped preamplifier. As a result, the peak power, output energy, and the conversion efficiency can be scaled up twice at least for the subsequent clad-pumped amplifiers.

2. Numerical Model

In the numerical study of laser dynamics, the pump absorption, the pulsed signal amplification, the cw amplified spontaneous emission (ASE), and the parasitic stimulated amplification were taking into account. The transverse coupling between radiated power and excited electrons in a single-mode fiber amplifier can be evaluated using a spatial overlapping factor under the assumption of uniform dopant concentration in the fiber core. The pulse amplification by cw and forward pumping can be described by the time-dependent 1-D convective equations. The simplified two-level coupled laser rate equations are considered according to the quasi-four-level ytterbium-doped laser system operating at 1064 nm. In this way, the amplification of a nanosecond laser pulse can be described by a set of governing equations as follows [17]:

$$\begin{aligned}\frac{\partial N_2(z,t)}{\partial t} &= \left[N_2(z,t)\left(\sigma_{\mathrm{a}}^{\mathrm{p}}+\sigma_{\mathrm{e}}^{\mathrm{p}}\right)-N_{\mathrm{t}}\sigma_{\mathrm{a}}^{\mathrm{p}}\right]\frac{P_{\mathrm{p}}^{+}(z,t)\Gamma_{\mathrm{p}}\lambda_{\mathrm{p}}}{hc_0A_0}-\frac{N_2(z,t)}{\tau_{21}}\\ &\quad-\sum_{i=0}^{C_1}\left[N_2(z,t)\left(\sigma_{\mathrm{e},i}^{\mathrm{s}}+\sigma_{\mathrm{a},i}^{\mathrm{s}}\right)-N_{\mathrm{t}}\sigma_{\mathrm{a},i}^{\mathrm{s}}\right]\frac{P_{\mathrm{s},i}^{+}(z,t)\Gamma_{\mathrm{s},i}\lambda_{\mathrm{s},i}}{hc_0A_0}\\ &\quad-\sum_{j=0}^{C_2}\left\{\left[N_2(z,t)\left(\sigma_{\mathrm{e},j}^{\mathrm{ASE}}+\sigma_{\mathrm{a},j}^{\mathrm{ASE}}\right)-N_{\mathrm{t}}\sigma_{\mathrm{a},j}^{\mathrm{ASE}}\right]\frac{\left[P_{\mathrm{ASE},j}^{+}(z,t)+P_{\mathrm{ASE},j}^{-}(z,t)\right]\Gamma_{\mathrm{ASE},j}\lambda_{\mathrm{ASE},j}}{hc_0A_0}\right\}\end{aligned}\tag{1}$$

TABLE 1
Parameters used in the ytterbium-doped fiber MOPA simulation

Symbol	Unit	Description	Value
N_t	m^{-3}	Doping concentration	3.33×10^{25} for 6/125 SM
N_1, N_2	m^{-3}	Population density at level 1 and 2	
σ_e^x	m^2	Emission cross section	2.79×10^{-25} at 1064 nm
σ_a^x	m^2	Absorption cross section	3.98×10^{-27} at 1064 nm
A_0	m^2	Core sectional area	2.83×10^{-11} for 6/125 SM
P_x	W	Instantaneous power	
Γ_x	---	MFD#-to-core overlapping factor	0.64 at 1064 nm
λ_x	nm	Wavelength	1064 for signal
c_0	$m\cdot s^{-1}$	Propagation speed in vacuum	3.0×10^8
n_x	$m\cdot s^{-1}$	Index of refraction in fiber	
α_x	m^{-1}	Propagation loss coefficient	9.44×10^{-3} ($\alpha_p=\alpha_s=\alpha_{ASE}$)
h	$m^2\cdot kg\cdot s^{-1}$	Planck constant	6.63×10^{-34}
τ_{21}	ms	Spontaneous lifetime	0.85
L	m	Active fiber length	2 for 6/125 SM
$C_1 / \Delta\lambda_1$	---	Channel number and bandwidth in Eq. (3)	30 and 1 nm
$C_2 / \Delta\lambda_2$	---	Channel number and bandwidth in Eq. (4)	40 and 2 nm
x =	p	s	ASE
	Pump	Signal	Amplified spontaneous emission

MFD is the mode field diameter.

$$\left[\frac{\partial}{\partial z}-\frac{n_p}{c_0}\frac{\partial}{\partial t}\right]P_p^+(z,t)=\left\{\left[N_2(z,t)\left(\sigma_e^p+\sigma_a^p\right)-N_t\sigma_a^p\right]\Gamma_p-\alpha_p\right\}P_p^+(z,t) \tag{2}$$

$$\left[\frac{\partial}{\partial z}-\frac{n_{s,i}}{c_0}\frac{\partial}{\partial t}\right]P_{s,i}^+(z,t)=\left\{\left[N_2(z,t)\left(\sigma_{e,i}^s+\sigma_{a,i}^s\right)-N_t\sigma_{a,i}^s\right]\Gamma_{s,i}-\alpha_{s,i}\right\}P_{s,i}^+(z,t), i=1,\ldots,C_1 \tag{3}$$

$$\left[\frac{\partial}{\partial z}\mp\frac{n_{ASE,j}}{c_0}\frac{\partial}{\partial t}\right]P_{ASE,j}^{\pm}(z,t)=\left\{\left[N_2(z,t)\left(\sigma_{e,j}^{ASE}+\sigma_{a,j}^{ASE}\right)-N_t\sigma_{a,j}^{ASE}\right]\Gamma_{ASE,j}-\alpha_{ASE,j}\right\}$$
$$\times P_{ASE,j}^{\pm}(z,t)+\sigma_{e,j}^{ASE}N_2(z,t)P_{SE,j},\quad j=1,\ldots,C_2 \tag{4}$$

$$P_{SE,j}\equiv mhv_{ASE,j}\Delta v_{SE}=mh\frac{c_0^2}{n_{ASE,j}^2\lambda_{ASE,j}^3}\Delta\lambda_2. \tag{5}$$

The boundary conditions in (6) at both fiber ends are

$$P_x^+(0,t)=R_0P_x^-(0,t)\quad\text{and}\quad P_x^-(L,t)=R_LP_x^+(L,t) \tag{6}$$

where R_0 and R_L correspond to the fixed reflectance at the input and output fiber ends. In the simulation, $R^0=0$ after the splice point and $R_L=10^{-6}$ for the angled-cleaved fiber end face.

The definition of the symbols and their corresponding values in the simulation are summarized in Table 1. Equation (1) is the two-level rate equation for determining the temporal population density at the upper energy level which is denoted as N_2. In addition, $N_t=N_1+N_2$ is the dopant concentration where N_1 is the population density of electrons at the lower energy level. C_1 and C_2 are the corresponding spectral channel numbers for pulsed parasitic stimulated emission and ASE. The numerical channel bandwidths ($\Delta\lambda_1$ and $\Delta\lambda_2$) and channel numbers (C_1 and C_2) affect

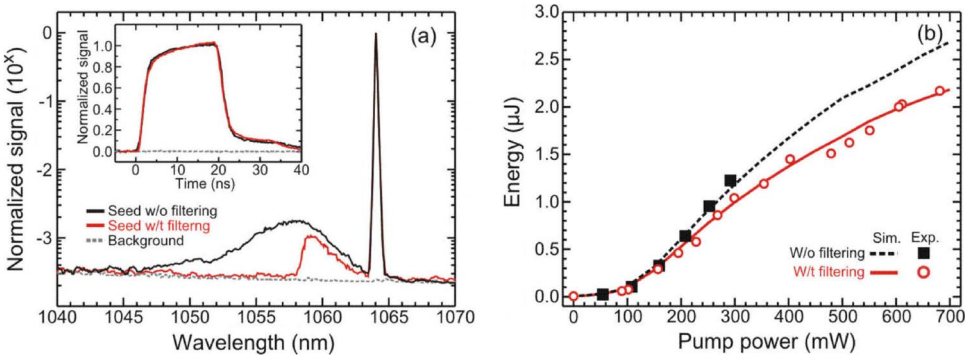

Fig. 1. (a) The measured input power spectra from the pulsed seed diode. The inset shows the corresponding temporal pulse shapes. (b) The measured and simulated output energies from the first-stage output at various pump powers with and without the insertion of the band-pass filter between the seed diode and the amplifier cascade.

whether the numerical results can converge to a pre-determined precision or not [17]. For ytterbium-doped fibers, the measured ASE without propagating through the active fiber is centered at 1026.8 nm with a bandwidth of 31 nm or 8.82 THz [18]. It is inhomogeneously-broadened in principle. Equations (2)–(4) describe the time evolution of cw pump power (P_{p}^{+}) in forward direction, signal peak power with a spectral profile $(P_{\mathrm{s},i}^{+})$ in the same direction with the pump, and cw ASE power $(P_{\mathrm{ASE},j}^{\pm})$ propagating in both forward and backward directions, respectively. Equation (5) depicts the contribution of cw spontaneous emission (SE) into the propagating laser mode, where $m = 1$ for the one polarization direction in a PM fiber [19], [20].

In Eq. (2), cw pump power at 976 nm is assumed in a single spectral channel with a linewidth of 1 nm. The signal peak power in Eq. (3) assumes a monochromatic signal pulse at 1064 nm due to a fiber Bragg grating (FBG) based signal frequency stabilizer used in the experiment. The amplified transient spike with the bandwidth spanning from 1035 nm to 1063 nm was measured. In order to reproduce the observed spike induced by the parasitic stimulated amplification, 30 discrete spectral channels with Gaussian profiles of bandwidth of 1 nm in Eq. (3) were used in the numerical model. The experimentally measured pulse shape as shown in the inset of Fig. 1(a) is used as the input pulse shapes in simulation. The cw ASE power in Eq. (4) was assumed to be generated within a bandwidth from 995 nm to 1074 nm, and is also decomposed into the multi-channels with Gaussian profiles. According to the measured emission cross section, the amplitude distribution of simulated cw ASE was obtained with the number and bandwidth of channel being 40 and 2 nm, respectively. The numerical results with good convergence were verified by the benchmark experimental results using the evolution of fluorescent spectra along the fiber in both propagation directions.

The rate equations are integrated using the central difference method in space and the fourth-order Runge–Kutta method in time. The modified Lax-Wendroff method was applied to solve the convective equations. For the simulations using multi-channel representation in spectral domain, the integration for ASE should be quantitatively corrected while numerically adjusting channel numbers and spectral bandwidths.

3. Parasitic Stimulated Amplification

Fig. 1(a) shows the measured power spectra of the original and filtered seed pulse. This core-pumped preamplifier operating at a repetition rate of 20 kHz was pumped forwardly at 976 nm and seeded at 1064 nm with an energy of ~8.8 nJ at a duration of 20 ns. There was a very weak broadband emission centered at 1058 nm associated the directly modulated seed diode laser (Lumics LU1064M010) with a single transverse mode. Even though a FBG was spliced at the distance of 50 cm from the laser diode for signal wavelength stabilization, these associated pulses still cannot be removed completely. The variation of the Fabry–Pérot laser diodes and the driving current profile could result in different levels of unwanted stray emission embedded in the input signal. Moreover, there was no discriminable difference between the original temporal shape and

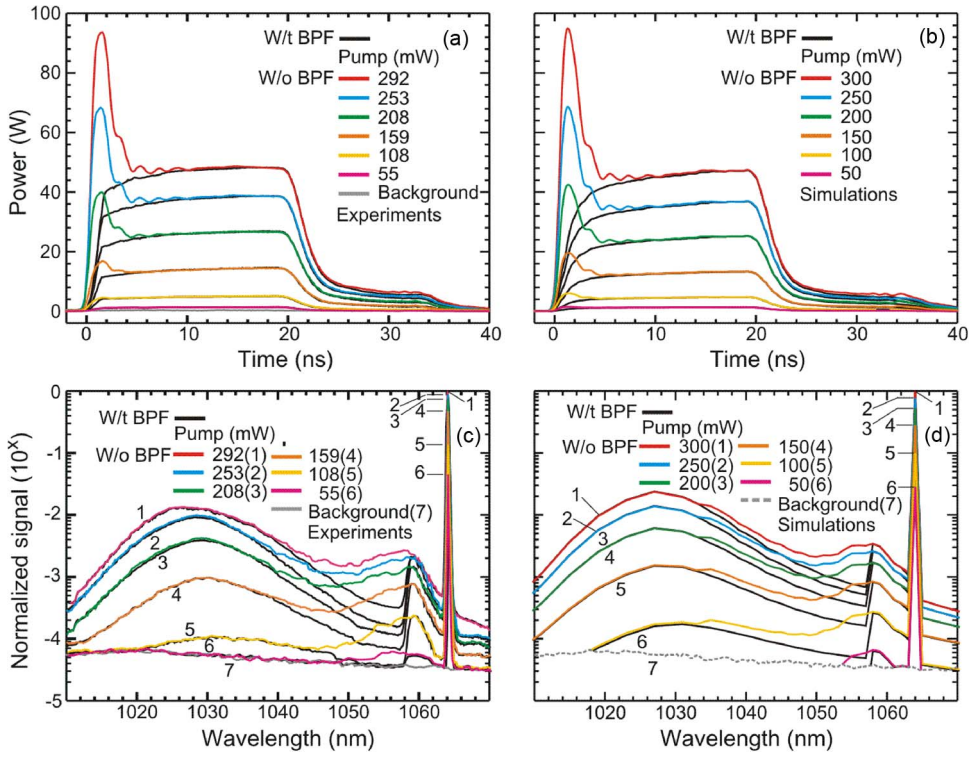

Fig. 2. Impact of the parasitic noise pulse in spectral domain. At the amplifier output, temporal pulse shapes of (a) experiments and (b) simulations, and the pulse spectra of (c) experiments and (d) simulations. The bandpass filter between laser diode seed and fiber amplifier has a bandwidth of 8 nm.

the filtered one when the stray emissions were removed, since the power ratio of the associated emission to signal is typically less than 5%. The standard fiber band-pass filter with a transmission bandwidth of 8 nm in full width at half maximum (FWHM) centered at 1064 nm is able to block the spectral components shorter than 1059 nm in wavelength. Fig. 1(b) shows the measured and simulated output energies generated from the core-pumped fiber preamplifier, which reveals that the amplified energy of the original input signal was about 20% higher than that of the filtered one. The pulsed noises in the original signal with shorter wavelengths experience a higher gain, because the difference in energy became larger as the pump power raises. Furthermore, good quantitative agreements between the experimental and numerical results can be obtained. In experiments, the FWHM linewidth of the 1064-nm signal and the 976-nm pump were 0.24 nm and $<$ 0.5 nm, respectively. Moreover, the original input pulse was amplified to only $\sim$1.3 μJ to avoid the serious shape deformation. Without the spike, the amplified energy as depicted by the hollow circles was only limited by the available core-pumped power and fiber nonlinear effects.

Fig. 2(a) shows the temporal pulse shapes measured at output of the core-pumped preamplifier. Formation of the leading spike was caused by the parasitic stimulated amplification of the input pulsed broadband emission, since the leading spike was removed when the emissions shorter than 1059 nm were filtered out. The measured peak power with the broadband spike was about 100 W, which was twice higher than that of the nanosecond signal when the core-pumped power exceeded 300 mW. When raising the core-pumped power, the peak power of amplified laser pulse with the spike is higher than twice that without the spike, and it is easy to grow to kilowatt power level. The simulated pulse shapes corresponding to Fig. 1(b) also support the arguments quantitatively as shown in Fig. 2(b). The slow-decay tail with $\sim$15 ns in duration at the trailing edge of the signal pulse was mainly contributed by the pulsed driver of the diode laser. Fig. 2(c) and (d) shows the corresponding spectra of Fig. 2(a) and (b), respectively. The spectral components of the spike can be identified to span from 1045 nm to 1063 nm. After filtering, the residual input noise was too weak

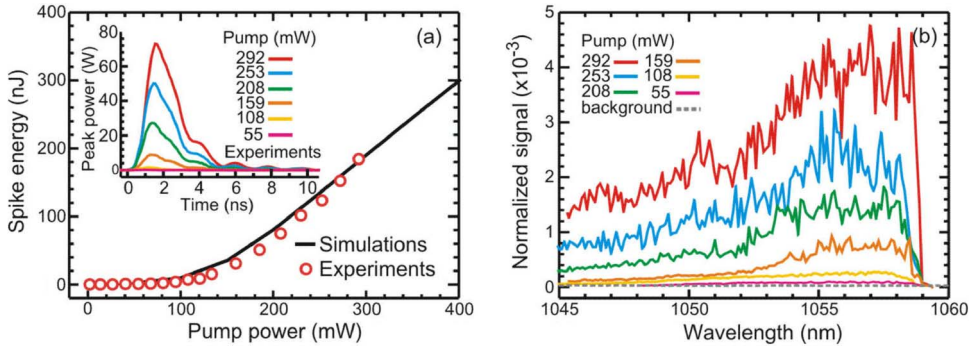

Fig. 3. The spike (a) energy and (b) measured spectral components at various pump powers. The inset in (a) shows the corresponding temporal shapes of spikes in experiment.

to be observed. Moreover, the spectral components centered at 1025 nm were mainly the cw fiber ASE generated by the residual stored energy in the core-pumped preamplifier, since a considerately low input energy is not able to extract a significant amount of the stored energy.

To focus on the spike itself in details, Fig. 3 shows the energies, shapes, and spectra of the amplified spike at various pump powers, which is derived from Fig. 1(b), Fig. 2(a), and Fig. 2(c), respectively. They were obtained by subtracting the measured amplified outputs without the spike from that with the spike. As shown in Fig. 3(a), the initial spike energy is too low to be detected at pump powers less than 100 mW. Although the spike experienced a higher gain due to the shorter wavelength, the amplifier slope efficiency for the spike was $\sim$1.1 μJ/W which is just about one-quarter of that for the 1064-nm signal in Fig. 1(b) at higher pump powers. It should be noted that the $\sim$2-ns pulse duration of the spike in the inset of Fig. 3(a) was limited by the photo detector bandwidth of 1 GHz. There is a small mutually coupled oscillation of the signal power and gain as shown in the inset of Fig. 3(a). The gain dependence of the spike can be confirmed as the signature of the parasitic stimulation amplification. Fig. 3(b) shows that the spectra of amplified spike centered near 1057 nm are broadband with a 3-dB bandwidth of 8.8 nm. It implies that the undesired spike may be recycled as a synchronized seed source to generate sub-nanosecond giant pulses.

To efficiently generate high peak power laser pulses with nanosecond width and millijoule energy at the output of power amplifier, it is essential to eliminate the leading spike in the diode-seeded preamplifiers. Fig. 4 shows the influence of the spike on the peak power scaling and conversion efficiency in the fiber MOPA system operating at 20 kHz. Considering 1 kW as the targeted peak power at output of the core-pumped preamplifiers, the attainable output energy without the spike is 2.5 times higher than that with the spike. In order to avoid the injection of cw fiber ASE, pulsed stray emission from the diode laser, and nonlinear spectral components originated from the preamplifiers to deplete the stored energy, a signal bandpass filter was inserted before the clad-pumped fiber amplifier. In this manner, the signal saturation in the clad-pumped amplifiers can only be caused by the 1064-nm signal. Moreover, the measured peak power was calibrated by making the integrated area under the pulse shape equal to the pulse energy. The pulse shape and repetition rate were measured by a fast detector. The pulse energy was derived from the average power measured by a thermal pile with repetition rates over kilohertz.

If the available core-pumped power and the signal depletion caused by the fiber nonlinear effects are not the problems in the preamplifier, the peak power and optical efficiency can be further scaled up. By decreasing the repetition rate and shortening the active and passive fibers, the measured peak power was scaled up to 3.5 kW at a 2-kHz repetition rate with a pulse energy of $\sim$40 μJ as shown in Fig. 4(c), but the conversion efficiency becomes one-third of the 20-kHz case. Such peak power level approaches the nominal damage threshold of $\sim$10 kW in a single-mode silica fiber. The distortion of pulse shapes shown in Fig. 4(c) is attributed to signal saturation, since the measured output energy is estimated to 2.1 times the signal saturation energy.

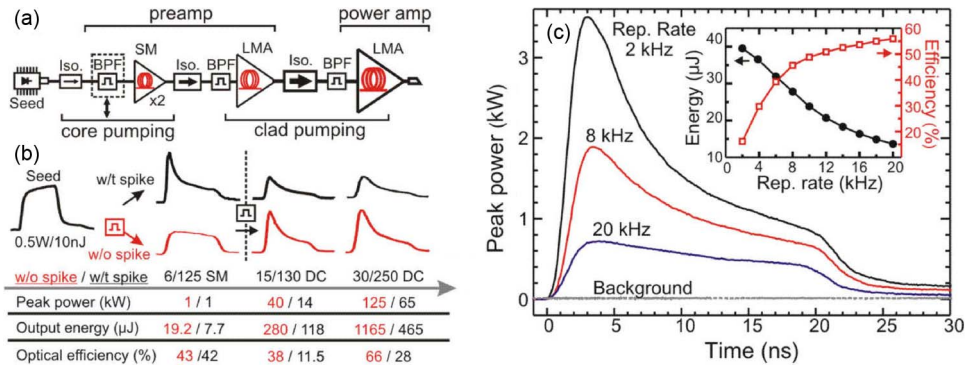

Fig. 4. (a) The experimental configuration of the multi-stage diode-seeded MOPA system. (b) The evolution of measured pulse shapes, peak powers, output energies, and conversion efficiencies stage by stage using a 20-ns and 20-kHz seed with and without the inter-stage band-pass filters (BPFs) in the core-pumped preamplifiers. (c) After removal of spike in experiments, the maximum energies and shapes limited by SRS at the output of core-pumped preamplifier by decreasing the repetition rate. The inset in (c) shows the output energy and efficiency at various repetition rates.

To scale up the peak power or pulse energy in a diode-seeded all-fiber MOPA system, it is crucial to raise the input of the 4th-stage power amplifier (30-μm core diameter), as well as the final output of the 3rd-stage power amplifier (15-μm core diameter). Without the harmful spike in the preamplifiers, we obtained the record-high energy of 280 μJ from the 15-μm output at 20 kHz compared to the previous studies [21]. As a result, the input energy of the 30-μm-core power amplifier reached one-third of its signal saturation energy for efficient energy extraction. So far, the power scaling of the power amplifier is limited by the damage threshold of fiber fuse [22].

4. Spectral and Gain Dependence of the Spike Formation

4.1. Spectral Dependence

There is a trade-off between high signal transmission and high ASEs blocking when deciding the pass bandwidth of filter. In simulation, the spectral width of the pulsed ASE can be studied independently. After amplification, the amplitude of transient spike is lower but the signal pulse shapes remain almost the same, as the input spectral width centered at 1064 nm is reduced in the normalized power spectra as shown in Fig. 5(a). The spectral components at shorter wavelengths contribute more peak power of the spike owing to the wavelength-dependent gain. Consequently, the corresponding spike-to-signal energy ratio increases from 0.5% to 16.5% when the spectral bandwidth of input window is increased from 2 to 30 nm.

The maximum output energy with an input energy of 3 μJ was obtained at 1030 nm as shown in the inset of Fig. 5(b). The corresponding lowest spike-to-signal energy ratio was $< 2\%$ at 1030 nm, which reveals the gain difference between the transient spike and the signal when the signal is small. Furthermore, the highest spike-to-signal energy ratio operating at 1030 nm and 1064 nm are 8.2% and 33% when the input energies are 3 μJ and 2 μJ, respectively. If the input energy further increases to its saturation level, the energy ratio at both wavelengths is getting lower, because the difference in the input energy for amplification can compensate that in the gain experienced. However, the energy ratio drops more rapidly if the input energy further decreases, because the cw ASE starts to significantly deplete the initial gain and affects the pulsed amplification of both signal and spike. This implies that the spike formation can be altered by adjusting the spectral window of the input pulse or the operating central wavelength.

4.2. Gain Dependence

The gain dependence of spike formation was numerically studied by varying the active fiber length or repetition rate for different pump absorptions or periods, respectively. When the active

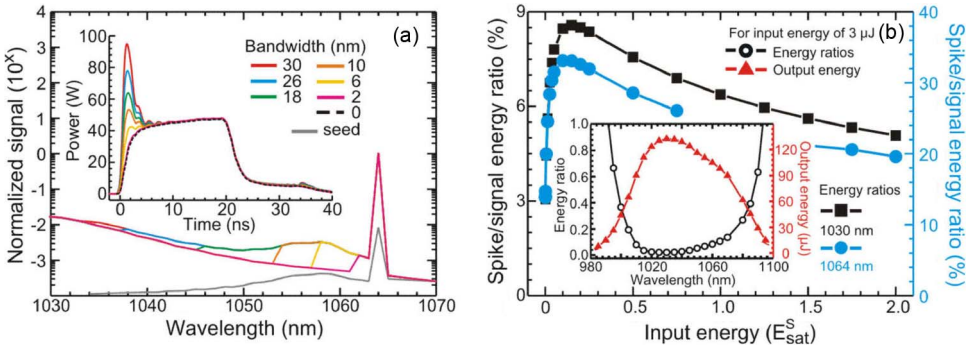

Fig. 5. Simulation of the spectral dependence of (a) BPF bandwidth and (b) signal energy. The spike-to-signal energy ratio at various input energies for the central wavelengths of 1030 nm (black squares on left) and 1064 nm (blue circles on right) are shown in (b). The inset in (a) shows the corresponding temporal pulse shapes at various BPF bandwidths. The inset in (b) shows the wavelength-dependent energy ratio and output energy for the same input energy of 3 μJ.

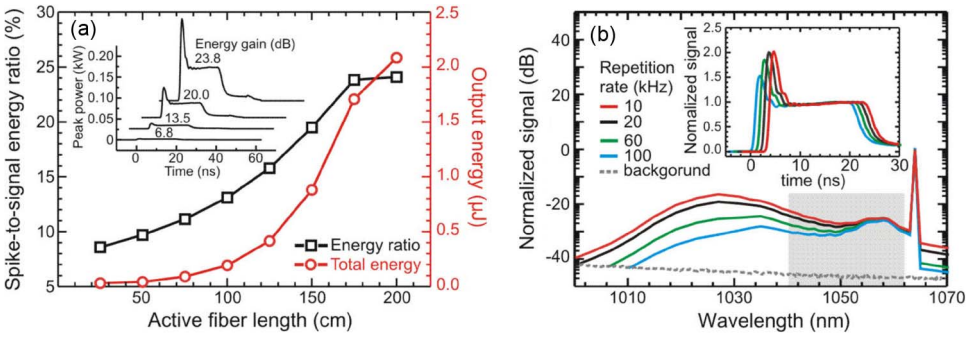

Fig. 6. (a) Simulation of the spike-to-signal energy ratio and the total output energy. The inset shows the corresponding pulse shapes and the amplification gains at 50, 100, 150, and 200 cm in active fiber length. (b) Output spectra of the spikes at various repetition rates. The inset shows the pulse shapes at 10, 20, 60, and 100 kHz in repetition rates with an artificial time delay of 1 ns to visualize the spikes clearly. The gray area in (b) marks the spectral range of the seed pulse stray emission.

fiber lengths are increased from 25 cm to 200 cm, Fig. 6(a) shows the spike-to-signal energy ratio increases from 8.5% to 24.1%, and the output total energy increases from 8.8 nJ to 2.1 μJ. Once the active fiber length is greater than 170 cm, the dopants could absorb almost all the pump power. The output energy and the spike-to-signal energy ratio start to saturate in spite of the gain difference between the signal pulse and the spike formation. The spike-to-signal energy ratio can be increased, if the complete pump absorption is achieved by a longer active fiber with a lower doping concentration. The reason is that the signal grows slower in the section of the active fiber near the output end, such that the weak input noise pulses have the chance to gain more energy.

As shown in Fig. 6(b), the simulated peak power of the leading spike is higher, as expected, if the repetition rate is decreased. The same trend of spike evolution was also observed in experiments. However, the corresponding response of the related spectral components is not apparent in the time-integrated power spectra due to the low spike-to-signal energy ratio. As the repetition rate is decreased, the amplitude of the forward cw ASE centered near 1030 nm also increases owing to the longer time interval between signal pulses for the cw ASE to grow.

5. Conclusion

We have experimentally and numerically studied the impact of the broadband pulsed stray emission of the seed and the cw fiber ASE in a diode-seeded fiber MOPA laser system. For a pulse-width-controllable nanosecond MOPA, the input pulsed stray emission from a seed diode laser should be

eliminated to scale up the available peak power or pulse energy efficiently. A peak power of >120 kW and an output energy of >1.2 mJ were obtained with a corresponding >63-dB energy gain and 56% conversion efficiency at 20 kHz from the nanosecond fiber MOPA. Through this investigation including the origin, formation, and suppression of parasitic stimulated amplification, it may help the fine correction of adaptive pulse shaping based on the direct current modulation to avoid the transient spike. Moreover, it is worthy of noting that the pulsed broadband emission with a FWHM bandwidth of 8.8 nm may also be served as a novel seed laser source for a fiber MOPA system. A sub-nanosecond giant pulse could be generated using a low-cost butterfly-packaged diode laser.

References

[1] D. J. Richardson, J. Nilsson, and W. A. Clarkson, "High power fiber laser: Current status and future perspectives," *J. Opt. Soc. Amer. B*, vol. 27, no. 11, pp. B63–B92, Nov. 2010.

[2] L. M. Frantz and J. S. Nodvik, "Theory of pulse propagation in a laser amplifier," *J. Appl. Phys.*, vol. 34, no. 8, pp. 2346–2349, Aug. 1963.

[3] M.-Y. Cheng *et al.,* "High-energy and high-peak power nanosecond pulse generation with beam quality control in 200-μm core highly multimode Yb-doped fiber amplifiers," *Opt. Lett.*, vol. 30, no. 4, pp. 358–360, Feb. 2005.

[4] T. Schreiber *et al.,* "Incoherent beam combing of continuous-wave and pulsed Yb-doped fiber amplifiers," *IEEE J. Sel. Topics Quantum Electron.*, vol. 15, no. 2, pp. 354–360, Mar./Apr. 2009.

[5] P. Dupriez *et al.,* "High average power, high repetition rate, picosecond pulsed fiber master oscillator power amplifier source seeded by a gain-switched laser diode at 1060 nm," *IEEE Photon. Technol. Lett.*, vol. 18, no. 9, pp. 1013–1015, May 2006.

[6] R. G. Smith, "Optical power handling capacity of low loss optical fibers as determined by stimulated Raman and Brillouin scattering," *Appl. Opt.*, vol. 11, no. 11, pp. 2489–2494, Nov. 1972.

[7] A. V. Smith and B. T. Do, "Bulk and surface laser damage of silica by picosecond and nanosecond pulse at 1064 nm," *Appl. Opt.*, vol. 47, no. 26, pp. 4812–4832, Sep. 2008.

[8] A. Malinowski *et al.,* "High power pulsed fiber MOPA system incorporating electro-optic modulator based adaptive pulse shaping," *Opt. Exp.*, vol. 17, no. 23, pp. 20 927–20 937, Nov. 2009.

[9] K. T. Vu *et al.,* "Adaptive pulse shape control in a diode-seeded nanosecond fiber MOPA system," *Opt. Exp.*, vol. 14, no. 23, pp. 10996–11001, Nov. 2006.

[10] J. Zhou, M. Gong, P. Yan, H. Zhang, and D. Wang, "Spike suppression in fiber amplifiers through nonlinear polarization rotation," *Opt. Lett.*, vol. 35, no. 9, pp. 1407–1409, May 2010.

[11] H. Li and K. Ogusu, "Dynamics behavior of stimulated Brillouin scattering in a single-mode optical fiber," *Jpn. J. Appl. Phys.*, vol. 38, no. 11, pt. 1, pp. 6309–6315, Nov. 1999.

[12] W. Zhao and E. Bourkoff, "Femtosecond pulse propagation in optical fibers: Higher order effects," *IEEE. J. Quantum Electron.*, vol. 24, no. 2, pp. 365–372, Feb. 1988.

[13] Y. J. Zhang, B. Q. Yao, Y. L. Ju, and Y. Z. Wang, "Gain-switched Tm^{3+}-doped double-clad silica fiber laser," *Opt. Exp.*, vol. 13, no. 4, pp. 1085–1089, Feb. 2005.

[14] J. Limpert *et al.,* "100-W average-power, high-energy nanosecond fiber amplifier," *Appl. Phys. B*, vol. 75, no. 4/5, pp. 477–479, Oct. 2002.

[15] J. Swiderski, D. Dorosz, M. Skorczakowski, and W. Pichola, "Ytterbium-doped fiber amplifier with tunable repetition rate and pulse duration," *Laser Phys.*, vol. 20, no. 8, pp. 1–6, Aug. 2010.

[16] A. Galvanauskas, M.-Y. Cheng, K.-C. Hou, and K.-H. Liao, "High peak power pulse amplification in large-core Yb-doped fiber amplifiers," *IEEE J. Sel. Top. Quantum Electron.*, vol. 13, no. 3, pp. 559–566, May 2007.

[17] Y. Wang, "Optimization of pulse amplification in ytterbium-doped double-clad fiber amplifier," *J. Lightw. Technol.*, vol. 23, no. 6, pp. 2139–2147, Jun. 2005.

[18] X. Peng and L. Dong, "Temperature dependence of ytterbium-doped fiber amplifiers," *J. Opt. Soc. Amer. B*, vol. 25, no. 1, pp. 126–130, Jan. 2008.

[19] C. H. Henry, "Theory of spontaneous emission noise and its application to lasers and optical amplifier," *J. Lightw. Technol.*, vol. LT-4, no. 3, pp. 288–297, Mar. 1986.

[20] A. A. Hardy and R. Oron, "Signal amplification in strongly pumped fiber amplifiers," *IEEE J. Quantum Electron.*, vol. 33, no. 3, pp. 307–313, Mar. 1997.

[21] C. Zheng *et al.,* "Single-mode MOPA structured all-fiber Yb-pulse fiber amplifier at low repetition," *Laser Phys.*, vol. 21, no. 6, pp. 1081–1084, Jun. 2011.

[22] R. Song, J. Hou, Y.-B. Wang, T. Liu, and Q.-S. Lu, "Analysis of the scalability of single-mode near-infrared supercontinuum to high average power," *J. Opt.*, vol. 15, no. 3, p. 035203, Mar. 2013.